Interstitial IgG antibody pharmacokinetics assessed by combined in vivo- and physiologically-based pharmacokinetic modelling approaches

Miro J. Eigenmann[1,2], Tine V. Karlsen[2], Ben-Fillippo Krippendorff[1], Olav Tenstad[2], Ludivine Fronton[1], Michael B. Otteneder[1] and Helge Wiig[2]

Author Affiliations: [1]Roche Pharma Research and Early Development, Pharmaceutical Sciences, Roche Innovation Centre Basel, Switzerland, [2]Department of Biomedicine, University of Bergen, Norway

Running title: Tissue interstitial pharmacokinetics of IgG antibodies in mice

Keywords: pharmacokinetics, interstitial space, PBPK model, lymph flow, monoclonal antibody, interstitial concentration, residual plasma, tissue distribution

Corresponding author: Miro J. Eigenmann
Schmiedgasse 27
4125 Riehen, Switzerland
miro.eigenmann@roche.com
ORCID: 0000-0002-7193-9264

Table of Content category: Computational Physiology and Modelling

Key point summary:

- For therapeutic antibodies, frequently, total tissue concentrations are reported representing a lump sum measure of antibody in residual plasma, interstitial fluid and cells. In terms of correlating antibody exposure to a therapeutic effect, however, interstitial pharmacokinetics might be most relevant.
- In this work we collected total tissue and interstitial antibody biodistribution data in mice and assessed the composition of tissue samples in order to correct total tissue measurements for plasma- and cellular content.
- All data and parameters were integrated into a refined physiologically-based

pharmacokinetic (PBPK) model for monoclonal antibodies in order to allow for a tissue specific description of antibody pharmacokinetics in the interstitial space.

- We found that antibody interstitial concentrations are highly tissue-specific and dependent on the underlying capillary structure but in several tissues reach relatively high interstitial concentrations contradicting the still-prevailing view that distribution to tissues and interstitial concentrations for antibodies are generally low.

Abstract

For most therapeutic antibodies, the interstitium is the target space. Although experimental methods for measuring antibody pharmacokinetics (PK) in this space are not well established, making quantitative assessment difficult, the interstitial antibody concentration is assumed to be low. Here, we combined direct quantification of antibodies in the interstitial fluid with a physiologically-based PK (PBPK) modelling approach with the goal of better describing the PK of monoclonal antibodies in the interstitial space of different tissues. We isolated interstitial fluid by tissue centrifugation, and conducted an antibody biodistribution study in mice, measuring total tissue- and interstitial concentrations in selected tissues. Residual plasma, interstitial volumes and lymph flows, which are important PBPK model parameters, were assessed *in vivo*. We could thereby refine PBPK modelling of monoclonal antibodies, better interpret antibody biodistribution data and more accurately predict their PK in the different tissue spaces. Our results indicate that in tissues with discontinuous capillaries (liver and spleen), interstitial concentrations are reflected by plasma concentration. In tissues with continuous capillaries (e.g. skin and muscle), ~50-60% of plasma concentration is found in the interstitial space. In brain and kidney, on the other hand, antibodies are restricted to the vascular space. Our data may significantly impact the interpretation of biodistribution data of monoclonal antibodies and might be important when relating measured concentrations to a therapeutic effect. Opposing the view that antibodies distribution to the interstitial space is limited, we show by direct measurements and model-based data interpretation that high antibody interstitial concentrations are reached in most tissues.

Abbreviations: BSA, bovine serum albumin; C_{ev}, extravascular concentration; C_{max}, maximal concentration; CO, cardiac output; C_{pla}, plasma concentration; C_{tis}, total tissue concentration; $fVec_{tis}$, tissue extracellular volume fraction; $fVint_{tis}$, tissue interstitial volume fraction; $fVrespla_{tis}$, tissue residual plasma volume fraction; EDTA, ethylenediaminetetraacetic acid; FcRn, neonatal Fc receptor; HSA, human serum albumin; IL17, interleukin 17; L_{tis}, tissue lymph flow; PBPK, physiologically based pharmacokinetic; PK, pharmacokinetics; PKPD, pharmacokinetic/pharmacodynamic;

Introduction

The importance of therapeutic antibodies in drug therapy has steadily increased over recent years. The pharmacokinetics (PK) of large molecules differs in many aspects from small molecule drugs as discussed in several recent reviews (Jones *et al.*, 2013; Ferl *et al.*, 2016; Wan, 2016). Nonetheless, distribution of antibodies in the sub-compartments (vascular, interstitial and cellular space) of different tissues is still not well-established in quantitative terms because experimental measurements at the sub-compartmental level of tissues are challenging. Therefore, most PK data for large molecules are reported as total tissue concentrations, however, this may not represent the effects driving concentration, but rather a mixture of vascular, intracellular and interstitial concentrations (Danhof *et al.*, 2007; Mouton *et al.*, 2008; Mariappan *et al.*, 2013). Notable differences in concentration levels are expected between the tissue sub-compartments (Lobo *et al.*, 2004; Wang *et al.*, 2008). Many therapeutic antibodies bind to targets on the cell surface and thus induce their therapeutic effect within the interstitial space of a tissue (i.e. the biophase) (Boswell *et al.*, 2012). Therefore accurate measurements or predictions of tissue interstitial concentrations are critical in order to estimate how much of the drug reaches the therapeutic target and evaluate the PKPD properties of therapeutic antibodies during drug development (Danhof *et al.*, 2007; Mariappan *et al.*, 2013).

So far, there is no broadly accepted gold standard method to experimentally assess antibody concentration in the interstitial space, i.e., at the target site (Wiig & Swartz, 2012). If total tissue concentrations are measured by ELISA or radiolabelling, subsequent corrections for residual plasma contamination and interstitial volume fractions of the underlying tissue might be applied in order to estimate the extravascular and interstitial tissue concentrations, respectively (Garg,

2007; Fronton *et al.*, 2014). Alternatively, PBPK models provide a robust tool for predicting the PK in the different tissue sub-compartments and can be further used to evaluate PK properties of compounds in development and to scale between different species or patient populations. They mathematically describe distribution of compounds throughout the body based on physiological processes, anatomical structures and physicochemical drug properties. Yet, because of the lack of physiological and quantitative knowledge surrounding driving processes for the biodistribution of large molecules, these models still contain a number of unknown physiological parameters which are required as inputs. This is also reflected by the diverse structure and parameterization of already published large molecule PBPK models (Covell *et al.*, 1986; Baxter *et al.*, 1994; Ferl *et al.*, 2005; Garg & Balthasar, 2007; Davda *et al.*, 2008; Urva *et al.*, 2010; Chen & Balthasar, 2012; Shah & Betts, 2012; Jones *et al.*, 2013; Fronton *et al.*, 2014). Further development and validation of large molecule PBPK models therefore require additional research to inform understanding of underlying distribution processes.

In this work, our objective was to investigate the PK of monoclonal antibodies in the interstitial space of individual tissues. Such knowledge would allow us to answer the question of how much of the administered therapeutic dose will reach the target site in a specific tissue. We herein report new biodistribution data, including measured interstitial concentrations in selected tissues, and parameter values forming the basis of a PBPK modelling approach, thereby providing new knowledge on tissue distribution and effect-driving concentrations of monoclonal antibodies. Our new findings are integrated into a PBPK model framework, enabling us to make antibody PK predictions at the target site in different tissues. Our data suggest high antibody exposure in the interstitial space of most organs, except the brain and kidney, and we show that often reported total tissue concentrations are much lower for many tissues than their interstitial concentrations. We demonstrate that an accurate assessment and interpretation of correction factors and input parameters are pivotal for the assessment of antibody PK. Importantly, our results clearly indicate that high interstitial concentrations can be achieved for antibodies in most tissues, which contradicts the prevalent assumption that therapeutic antibody concentrations in this space are low.

Materials & Methods

Ethical approval

All *in vivo* studies were carried out in accordance with the regulations of the Norwegian State Commission for Laboratory Animals in agreement with the European Convention for the Protection of Vertebrate Animals used for Experimental and Other Scientific Purposes and Council of Europe (ETS 123) and approved by the AAALAC International Accredited Animal Care and Use Program at University of Bergen. The authors also confirm to be compliant with the ethical principles under which The Journal of Physiology operates and to adhere to the Animal Ethics Checklist presented in the editorial by Grundy (Grundy, 2015).

Animal studies

FVB/NhanHsd mice supplied by Envigo (An Venray, Netherlands) were used for all *in vivo* measurements. For every study, both sexes were used (total of 34 females and 26 males). The body weights ranged from 19-34 g with a mean of 23 g and the age of the animals ranging from 8-12 weeks. The mice were fed *ad libitum*. During invasive experimental procedures, the animals were anesthetized with 1.5% isoflurane (IsoFlo®Vet 100%, ABBOTT Laboratories Ltd, England) in 100% O_2. The depth of anaesthesia was monitored by testing the withdrawal reflexes (paw). During anaesthesia, the body temperature was kept stable using a servo-controlled heating pad and rectal probe. At the end of the experiment, animals were euthanized by cervical dislocation.

Radiolabelled probes

We used various radiolabelled compounds in our *in vivo* studies. ^{51}Cr-ethylenediaminetetraacetic acid (EDTA) (produced by GE Healthcare Limited, delivered by IFE, Institute for Energy Technology, Norway) was utilised for assessment of extracellular spaces. Human serum albumin (HSA) and anti-interleukin 17 (IL17) IgG were labelled with 125-iodine using Iodo-Gen as described in detail previously (Wiig *et al.*, 2005). In summary, a solution of 5 mg 1,3,4,6-tetrachloro-3α,6α-diphenylglycouril (Sigma-Aldrich Co., product number T0656) in 5 mL chloroform was prepared and 0.1 mL transferred into a 1.8 ml Nunc vial (Nunc-Kamstrup,

Roskilde, Denmark). Chloroform was evaporated under nitrogen forming water-insoluble Iodo-Gen in the Nunc vial. One and a half mg of compound was added to 1 mL 0.05 M PBS with15 µL 0.01 M NaI and 10 MBq ^{125}I (Institute for Energy Technology, Kjeller, Norway). The vial was gently mixed for 10 min before the solution was removed. The tracer solution was dialysed against 1 L of 0.9% of saline and 0.02% azide to remove unincorporated isotope. The labelled probes were additionally purified prior to each intravenous injection using a 40 kDa cut-off spin filter (Amicon). Separate terminal plasma and urine samples were collected during the study and tested for free iodine and purity using spin filters and high-through put liquid chromatography (HPLC).

Biodistribution study

Concentrations of ^{125}anti-IL17 IgG were measured in plasma and 11 tissues (adipose, bone, brain, gut, heart, kidney, liver, lung, muscle, skin and spleen) at 10 time points with three mice at each time point. Sampling times were 10, 30 and 90 min, 3, 6 and 12 h and 1, 2, 5 and 15 d, with the focus being on early time points in order to resolve the early tissue distribution phase. A dose of 10 mg/kg was administered i.v. through the tail vein. For terminal tissue sampling, mice were anaesthetized; a blood sample was retrieved from the tail vein using heparinized glass capillaries followed by euthanasia. Plasma was isolated by centrifugation of the blood sample for 10 min at 1000 g. Harvested tissue samples were blotted dry on a paper tissue to remove surface blood. Separate samples for skin and muscle were obtained in order to isolate interstitial fluid by tissue centrifugation. Samples were weighed, transferred to vials and radioactivity was determined in a gamma-counting system (Wallac Wizard 1470 gamma counter, PerkinElmer). An additional blood sample was taken at several time points and filtered through a spin filter (40 kDa cut off) in order to determine the amount of free iodine in the system. The amount of drug was assessed based on specific activity of the probe and correction for radioactive decay. Drug content in tissues is reported per gram wet weight of the respective tissue. The tissue sample volumes (V_{tis}) were calculated based on the measured sample weights:

$$V_{tis} = \frac{Weight}{Density} \quad (1)$$

A density of 1 g/cm^3 was assumed for all tissues, except 0.92 and 1.3 g/cm^3 for adipose and bone, respectively (Brown *et al.*, 1997; Valentin, 2002). This permitted us to derive the total tissue concentrations.

Tissue centrifugation

Interstitial concentrations

A preliminary study was performed to test the isolation of native interstitial fluid using the tissue centrifugation technique (Wiig *et al.*, 2003) from 11 tissues (adipose, bone, brain, gut, heart, kidney, liver, lung, muscle, skin and spleen) and evaluate the plasma admixture and dilution by intracellular fluid in the centrifugate of each tissue. Based on the obtained data, muscle and skin were selected to establish interstitial PK during the biodistribution study as these tissues allowed collection of relatively pure interstitial fluid with limited plasma and intracellular fluid contamination. To avoid evaporation, all procedures were performed in a humidity chamber (98% relative humidity). Tissue samples were placed on a mesh in an Eppendorf tube and centrifuged at low speed of 424 g for 10 min. After centrifugation, the tubes were immediately transferred back to the humidity chamber where isolated fluid samples at the bottom of the tube were transferred into a tube containing 500 µL of saline and counted in the gamma counter to measure the ^{125}anti-IL17 IgG content in the centrifugate.

Tissue volume fractions

Extracellular space by ^{51}Cr-EDTA

The time needed for tracer equilibration was tested in preliminary studies. Under anaesthesia, two 1 cm incisions penetrating the skin and muscle layer were made lateral from the spine and below the rib cage, and the kidney pedicles were tied off to prevent tracer excretion. Following wound closure, ^{51}Cr-EDTA (~16.6 kBq in 100 µL) was injected i.v. into the tail vein of seven mice. Serial blood sampling from the tail vein after 30, 60 and 90 min revealed that tracer levels in plasma were not different at these time points. Although this suggests that the tracer was equilibrated already at 30 min, we chose the 60 min equilibration time for the extracellular tracer to ascertain complete equilibration. In a group of six mice, ^{51}Cr-EDTA was injected as described

before. The mice were kept under anaesthesia for 60 minutes before a terminal blood sample was withdrawn and the animals were euthanized. Subsequently, adipose tissue, bone, brain, gut, heart, kidney, liver, lung, muscle, skin and spleen were harvested. Surface blood was removed by briefly blotting tissues on a paper tissue. All samples were weighed, transferred to counting tubes and counted in the gamma counter. The tissue extracellular volume fraction (*fVec*$_{tis}$) was calculated as:

$$fVec_{tis} = \frac{^{51}Cr\ counts/g\ tissue}{^{51}Cr\ counts/mL\ plasma} \quad (2)$$

Residual plasma space by ^{125}I-HSA

After anaesthesia, six mice received an i.v. bolus injection of ^{125}I-HSA (~17 kBq in 100 µL) that was allowed for a 5 min distribution time, sufficient to distribute in but not to extravasate from plasma (with few exceptions, as described in what follows) before blood sampling and euthanasia. Thereafter, tissues were harvested, blotted dry and transferred to the gamma counter. Importantly, no other measures to remove additional blood were employed. Residual plasma fractions (*fVrespla*$_{tis}$) in harvested tissues were calculated as follows:

$$fVrespla_{tis} = \frac{^{125}I\ counts/g\ tissue}{^{125}I\ counts/mL\ plasma} \quad (3)$$

Interstitial volume fractions

We used our measured volume fractions to derive a tissue interstitial volume fraction (*fVint*$_{tis}$) based on the following relationship:

$$fVint_{tis} = fVec_{tis} - fVrespla_{tis} \quad (4)$$

Lymph flow measurements

To measure the lymph flow in muscle and skin, Alexa 680-labelled macromolecular tracers were injected intradermally and intramuscularly in the hind paw and thigh of mice respectively. Washout rates of the tracer from the injection site were assessed by optical imaging using the Optix MX system to measure the fluorescent signal. The rates were computed based on the

monoexponential reduction of the fluorescent signal as described in detail previously (Karlsen *et al.*, 2012). In short, we fluorescently labelled bovine serum albumin (BSA), anti-IL17 IgG antibody and a Triple-A mutant (neonatal Fc receptor (FcRn) non-binding) antibody with the near infrared Alexa680 fluorophore with an antibody labelling kit (SAVI^{TM} Rapid Antibody Labelling Kit, Invitrogen). The three different macromolecular tracers were employed to check for a possible effect of molecular weight (BSA vs. anti-IL17 IgG) and FcRn binding (anti-IL17 IgG vs. FcRn non-binding IgG) upon removal from the interstitial space. Volumes of 0.5 µL of tracer were injected with a 34G Hamilton syringe. After a 60 min distribution phase, five measurements were taken with 1 h intervals. Animals were anesthetized during imaging, but awake and freely moving in between the measurements to assess washout of normally active animals, knowing that immobility reduces lymph flow (Lindena *et al.*, 1986; Modi *et al.*, 2007). For each tracer and tissue the washout was assessed in six individuals. Optix Optiview software was used to analyse the images. Flow values were subsequently derived by multiplying removal rates from the interstitial volume of the respective tissue:

$$Ltis = fVint_{tis} \times V_{tis} \times k, \quad (5)$$

where *Ltis* it the tissue lymph flow, *fVint* the interstitial volume fraction, *Vtis* the tissue volume and *k* the measured tracer removal rate.

Corrections of total tissue concentrations

During the biodistribution experiments, plasma and total tissue concentrations were measured. Extravascular tissue concentrations were derived by subtracting the amount of antibody in the residual plasma from the measured total amount found in tissue and dividing what remained by the extravascular tissue volume (Garg, 2007; Fronton *et al.*, 2014):

$$C_{ev} = \frac{C_{tis} \times V_{tis} - C_{pla} \times Vrespla_{tis}}{V_{tis} - Vrespla_{tis}} \quad (6)$$

C_{ev} represents the tissue extravascular concentration, C_{tis} the experimentally assessed total tissue concentration, C_{pla} the plasma concentration and V_{tis} the experimentally measured total tissue sample volume. $Vrespla_{tis}$ is the residual plasma volume in the respective tissue sample and is

determined based on the corresponding measured residual plasma fraction multiplied with the total sample volume. Residual plasma fractions utilised for correction were based on the ^{125}I-HSA distribution. Under the same assumptions, we additionally used the measured amount of anti-IL17 IgG in tissues after 10 min in the biodistribution study for residual plasma corrections.

Statistics

Mean and standard deviation (SD) are reported for measured data. For comparison of groups a two-tailed Student's t-test or one-way analysis of variance (ANOVA) was conducted. $P \leq 0.05$ was considered statistically significant. Analyses were performed in GraphPad PRISM version 6.0.

PBPK modelling

We integrated and evaluated the newly measured biodistribution data and parameter values in a PBPK modelling approach. The model was coded in the Simbiology toolbox in MATLAB R2016a and was used to fit total tissue- and, where available, interstitial concentrations. Tissue distribution , lymph flows (except for the muscle and skin), systemic plasma volume, systemic clearance and interstitial accessible volume for the skin and muscle were estimated using the fminsearchbound and lsqnonlin algorithms, whereas other parameters were fixed to reported values (Shah & Betts, 2012). The herein measured physiological parameter values (i.e. residual plasma- and interstitial volume fractions and lymph flow in the skin and muscle) were utilised as input parameters for the model and limited to a range of measured values ± 20% during the estimation to permit variability. The presented model integrated only well-established or required parameters and mechanisms in order to describe our data and allow prediction of the concentrations in the different tissue sub-compartments. For this analysis we avoided, wherever possible, including parts into the model structure where no experimental data were available and which were not directly affecting our research question (e.g., detailed endosomal compartment, FcRn receptor, target binding, etc.). Furthermore, as all major organs were sampled and included within the model structure, making up for 92% of the body weight and 95% of the cardiac output. Therefore, no additional carcass or rest of body compartment was included. This is not expected to cause a relevant impact or bias in terms of amount of antibody distributed to the included organs.

Tissue distribution space, inflow and removal of antibodies were modelled differently for the individual tissues based on their capillary structure. Tissues with continuous capillaries provide a distinct separation of vascular and interstitial space for macromolecules. Therefore, tissue distribution, representing a lump sum of convective flow and reflection coefficient, and removal (i.e., lymph flow) was estimated. Tissues with especially tight and size-selective capillaries (blood brain barrier and glomerular filter of the kidneys) were modelled solely by the vascular space because macromolecules are assumed to be restricted here and the measured amount in tissue is entirely explained by the extent of the residual plasma content. Thus, no distribution to the interstitial space or lymph removal was accounted for with these tissues. In the case of tissues with discontinuous capillaries, the vessel wall does not provide a clear separation of vascular and interstitial space for IgGs and the two spaces equilibrate rapidly, therefore interstitial concentration is assumed to reach plasma concentration levels within a few minutes. As such, in these tissues the distribution space was modelled as one lumped space containing the vascular and interstitial compartment. Antibody drugs enter this space by arterial blood flow and are removed by venous blood- and lymph flow that can, however, not be distinguished based on the data. An exclusion volume in the interstitial space of the skin and muscle was estimated based on the measured interstitial volumes and PK data. Tissue-intrinsic clearances were integrated based on previously published contribution of tissue clearances to the total plasma clearance (Eigenmann *et al.*, 2017). A schematic representation of the model is found in Figure 1 and the model equations are presented in the Appendix. After fitting the PBPK model to the biodistribution data and parameter estimation, the model was utilised in order to simulate the PK in the tissue sub-compartments of the individual tissues. The PBPK model source code (Simbiology file) and a MATLAB-script which enable running and plotting the simulations based on the model and parameter values we present in this work was provided as supportive information.

Results

Antibody biodistribution study

To assess the normal antibody distribution, we first conducted an anti-IL17 IgG biodistribution

study in normal FvB mice. The biodistribution data, including plasma and tissue PK profiles are presented in Figure 2. The measured concentrations represent total tissue concentrations. After an i.v. dose of 10mg/kg, a plasma PK biphasic profile was observed. Maximal concentration (C_{max}) was 215ug/mL followed by a fast decline in concentration, which indicated the tissue distribution phase. Total tissue concentrations were mostly >1 order of magnitude lower than the plasma concentration. Well-perfused organs like the heart, kidney, liver, lung and spleen had generally higher total concentrations, while lower concentrations were determined in adipose, bone and muscle. Over the time course of the entire study, negligible free iodine was measured (<0.4%) within the system.

Tissue centrifugation – interstitial concentrations

In order to measure interstitial concentrations in the skin and muscle and compare them to the respective total tissue PK we isolated native interstitial fluid from the muscle and skin by tissue centrifugation and directly assessed anti-IL17 IgG interstitial concentrations. In the centrifugate the plasma content and intracellular dilution was assessed by ^{125}I-albumin and ^{51}Cr-EDTA centrifugate-to-plasma ratios. Residual plasma fraction of 0.065 and 0.056 were measured in the centrifugate for skin and muscle respectively. ^{51}Cr-EDTA tissue-to-plasma ratios of ~1.12 and ~0.79 were found for the skin and muscle, respectively, indicating slight contamination by intracellular fluid in the muscle centrifugate. The biodistribution data in the centrifugate were corrected for these factors. The interstitial PK profiles for both tissues are depicted in Figure 3. In each, a C_{max} of about 45 ug/mL was observed corresponding to ~50% of the plasma concentration after reaching C_{max}. This indicates high interstitial exposure for antibodies in the skin and muscle. Compared to the measured, corresponding total tissue concentrations, the interstitial concentration is >10 times or >3 times higher for muscle and skin, respectively.

Tissue volume fractions

In a next step, we assessed residual plasma and interstitial fluid per gram of tissue to attribute the total amount of measured drug in the tissue sample to the various tissue sub-compartments. Residual plasma and extracellular volumes were established by tracer distribution, whereas interstitial volumes could be derived by subtracting the residual plasma from the total

extracellular space. These volume fractions are important input parameters in the PBPK model and are necessary to more accurately describe distribution to and within the individual tissues.

Extracellular tissue volumes were assessed using a ^{51}Cr-EDTA tracer and measuring its distribution volumes in tissues 60 min after injection. Extracellular volumes were derived for all tissues and individual volumes, mean and standard deviation are located in Figure 4a. The highest mean extracellular volume fraction of 0.45 was found for the skin. No measurements are available for brain (blood brain barrier) and kidneys (tied off because of excretion). Residual plasma fractions assessed from the 5 min distribution space of ^{125}I-HSA are summarized in Figure 4b. High residual plasma volumes were found for the lung, kidney, liver, heart and spleen, whereas they were lower in the bone, gut, skin brain, muscle and adipose. It is of note, however, that in tissues with leaky, discontinuous capillaries (i.e., liver, spleen and bone marrow), tracer likely extravasated, therefore resulting in an overestimation of the local plasma volume.

We calculated the interstitial space volume in tissues by subtracting the residual plasma from the extracellular fluid fraction. As evident from Table 1, the skin interstitial volume fraction of 0.431 was by far the highest. In contrast, the lowest interstitial volume fraction of 0.093 was found in adipose tissue. In other tissues, corresponding volume fractions were in the range of 0.12 – 0.24. Overall, the fractional volumes (extracellular, residual plasma and interstitial) could be measured with strong precision. Exceptionally, adipose tissue had a rather high coefficient of variation (42.9-47.8 %). All volume fractions and coefficients of variation are summarized in Table 1.

Corrections of total tissue concentrations

Extravascular tissue concentrations derived by subtracting the amount of antibody in the residual plasma from the total tissue concentrations are reported in Figures 5 and 6. Therein, the impact is portrayed in terms of residual plasma contamination in the different tissues on the measured antibody content in total tissue samples and the importance of accounting for it when interpreting total tissue measurements. The blue shaded areas are derivative of correcting for residual plasma fractions as measured based on tissue distribution of labelled HSA and anti-IL17 IgG after 5 and 10 min of distribution time, respectively. As evident from Figure 5, there was a more profound influence of residual plasma volume correction in highly perfused tissues, like the lung and heart,

versus the lesser perfused adipose, gut, muscle and skin.

The same correction approach was applied for bone, brain, kidney, liver and spleen (Figure 6), though it is seen that in these tissues, the entire amount of the drug appears to be in the measured ^{125}I-albumin- or very early anti-IL17 IgG distribution spaces. After subtraction of the amount of drug within these spaces, the anticipated concentration range approximates towards zero.

Lymph flow in muscle and skin

Lymph flow is a critical parameter for antibody biodistribution because it represents the exit route for macromolecules from the interstitial space back to the plasma. This parameter was assessed in muscle and skin based on near-infrared labelled BSA, anti-IL17 IgG and FcRn non-binding IgG. We investigated whether there was an influence of molecular size, between 66.4 kDa and 150 kDa, and of FcRn binding on the macromolecular washout from the tissue interstitial space. A size-dependent hindrance in accessing lymph vessels would appear as a faster removal rate for labelled BSA compared with IgG antibody. If FcRn-based transcytosis were an alternative means for antibodies to leave the tissue interstitial space, the FcRn non-binding antibody would have a lower washout rate than anti-IL17 IgG with normal FcRn binding. The measured removal rates for skin and muscle for the three macromolecules are presented in Figure 7.

No statistically significant differences in washout of the three different tracers were found using one-way ANOVA (p-values of 0.5 and 0.6 for skin and muscle respectively), indicating no influence of molecular weight and FcRn-based transcytosis on the measured removal rate. The actual flow values were determined by multiplying the mean removal rates (Figure 7) with the interstitial tissue volume (Table 2) that was assessed earlier in this work in accordance with equation 5. The lymph flow derived for skin was 0.633±0.134 mL/h, and for muscle, it was 0.162±0.052 mL/h.

PBPK modelling

The available data and parameter values were integrated into the PBPK model and PK in the different tissue sub-compartments described. This enabled estimation of the remaining

biodistribution parameters for monoclonal antibodies and the model could subsequently be used for predictions of antibody PK in different tissue sub-compartments following alternative dosing schedules, with potential value as a tool for translation to other species. The final model fostered a good description of the biodistribution data and PK in the different tissue sub-compartments (interstitial and vascular). Model parameters were precisely estimated. The parameter values in the final model are displayed in Table 2.

Model fits and the prediction of drug content per gram of tissue in the various tissue sub-compartments for all analysed tissues are depicted in Figure 8. For tissues with discontinuous capillaries (liver and spleen), the vascular and interstitial space cannot be discriminated as a consequence of the quick exchange in these spaces. Interstitial concentrations are expected to follow that of plasma. In tissues with very tight or size-selective capillaries (blood brain barrier, glomerular filter of the kidneys), antibodies are expected to be restricted to the vascular space and no or negligible interstitial concentrations are predicted. In these cases, lymph flow and distribution to the tissue interstitial space cannot be determined using model estimation, and the measured interstitial volume fraction not be employed as an input value. The interstitial concentrations measured in the skin and muscle were well-described by the model featuring an estimated interstitial exclusion of 37% and 25%, respectively.

The sensitivity of simulated PK profiles on perturbations on individual parameters was evaluated. Changes in tissue-specific parameters did not significantly affect the PK in different tissues. Altering the systemic plasma clearance had a great impact on the elimination phase for all tissues. In the liver, spleen, brain and kidney varying the vascular or lumped vascular/interstitial volume fractions strongly affected the level of the simulated PK profile. In tissues with continuous capillaries, parameter sensitivity was high for interstitial and vascular volume fractions, thereby modifying the concentration level. Altering the lymph flow and tissue distribution flow in these tissues, on the other hand, notably affected the concentration level while also having an effect on the kinetics (i.e., time when maximal concentration is observed). Generally insignificant sensitivity was observed for tissue plasma flows. The calculated sensitivities for each parameter, averaged over the simulated time-course, are summarized in a sensitivity matrix depicted in Figure 9.

Discussion

In this work, we investigated determinants of tissue distribution and biophase concentrations of therapeutic antibodies in different tissues using: (i) tissue centrifugation to directly assess interstitial concentrations; and (ii) correction of total tissue concentrations and the related impact on PBPK modelling. Also, early time points (i.e., 10, 30 and 90 min) were sampled during the antibody biodistribution study, in order to garner insights into tissue distribution within the individual tissues.

In terms of total tissue concentrations, our results are in strong agreement with previous published antibody biodistribution studies, which can be seen first-hand when comparing the antibody biodistribution coefficients with those compiled by Shah et al. (Shah & Betts, 2013). Additionally, base distribution parameters, volume of distribution (1.25 mL) and systemic clearance (8.6 mL/d/kg), were all within the expected range (Deng *et al.*, 2011). Important differences are notable, however, when reviewing the expected extravascular and interstitial concentrations. Here, we showed high interstitial antibody exposure to target cells in muscle and skin with concentrations up to 50% of the plasma concentration. For large molecules, corrections for drug in residual plasma are frequently performed in order to calculate extravascular concentrations. Interestingly, these corrections, with residual plasma of the respective tissues measured by ^{125}I-HSA and ^{125}anti-IL17 IgG distribution space, resulted in negligible anticipated extravascular concentrations in brain and kidney. This is probably explained by the very tight capillaries constituting the blood brain barrier and the size-selective fenestrated capillaries in the glomerular filter. Both types of capillaries practically prevent IgG antibodies from entering the tissue space. Further, with regards to the liver, spleen and bone, the zero line was included after correcting for the amount of drug in the distribution space of the macromolecular tracer. For these tissues, however, the interpretation of this finding would be the opposite. These tissues possess discontinuous capillary walls that are non-restrictive to proteins (Rippe & Haraldsson, 1994; Sarin, 2010). Therefore, the measured space with the macromolecular tracer used for correction most probably represents a mix of the plasma and interstitial space. Correcting for the amount of drug in that space should therefore not be performed to calculate extravascular concentrations in such tissues. Our results actually suggest that the tracer is equilibrated in these

organs at between 5 to 10 min of circulation time. As a result of this facilitated exchange with the plasma space, the extravascular space of tissues, with discontinuous capillaries, might be interpreted as extended plasma spaces. This finding leads to the assumption that interstitial concentrations in tissue with discontinuous capillaries are reflected by the plasma concentration. Overall, our results provide evidence that total tissue concentrations are much lower than the actual interstitial concentrations in tissues (except in the brain and kidneys). Therefore, our findings contrast with the common notion in the pharmacological literature that interstitial concentrations are generally much lower than vascular concentrations (Lobo *et al.*, 2004; Wang *et al.*, 2008). On the other hand, they are in line with earlier published pre-nodal lymph to plasma concentration ratios of macromolecules in various tissues (e.g., (Aukland & Reed, 1993; Michel & Curry, 1999), where pre-nodal lymph can be expected to be representative for interstitial fluid in steady state conditions.

Distribution spaces for ^{125}I-HSA- and chromium EDTA were measured with robust precision. The residual plasma fractions based on HSA distribution were systematically higher than previously reported (Garg, 2007; Boswell *et al.*, 2014). These previous values are based on the distribution of red blood cells. In such cases, a systemic haematocrit value is regularly employed used to derive the residual plasma volumes in tissues. Yet, it is well-established that the local haematocrit in the smaller tissue vessels might be considerably lower than the systemic haematocrit, known as the "Fåhræus Lindqvist effect" or the "screening effect" (Goldsmith *et al.*, 1989; Fung, 1993). Therefore, utilising systemic haematocrit values to derive residual plasma fractions based on red blood cell fractions will erroneously lead to lower correction factors, thereby introducing a systematic bias. The quantitative importance of such bias is illustrated in Figure 10, where there is the comparison of the PK profiles for the analysed tissues, including residual plasma corrections based on red blood cell distribution (Garg, 2007; Boswell *et al.*, 2014) and based on ^{125}I-HSA and ^{125}anti-IL17 IgG distribution after 5 and 10 min of circulation time, respectively. A direct assessment of the plasma space is hence, in our opinion more representative with the exception of organs with discontinuous capillaries, where the tracer will quickly extravasate and equilibrate in the entire extravascular phase as discussed earlier. Extracellular volume fractions measured by ^{51}Cr-EDTA distribution are also in solid agreement

with previous literature (Pierson *et al.*, 1978; Tsuji *et al.*, 1983; Boswell *et al.*, 2014), especially considering the different properties of the applied tracers. These findings show that corrective factors have a major impact on estimated extravascular concentration, thus demonstrating the significance of exact measurements as possible and careful interpretation of the results. A critical evaluation of the used tracer is therefore warranted with such values as fixed input parameters in a PBPK model.

Lymph flow plays an important role in the biodistribution of therapeutic antibodies because of its involvement in the transport of filtered macromolecules from the interstitium back to the systemic blood circulation (Wiig & Swartz, 2012). As such, it is a critical parameter in most large molecule PBPK models. However, the input values used for tissue lymph flow in different published PBPK models vary by a factor of up to ~5000 times and no systematic measurement values are available (Ferl *et al.*, 2005; Fronton *et al.*, 2014). Here, we derived tissue lymph flow values in the muscle and skin based on macromolecular washout in order to directly use measured values in PBPK models. Integration of both measured lymph flow values result in an adequate description of the biodistribution data. Optimized lymph flow values by model-based parameter estimation would, however, be lower in the skin (0.15 vs. 0.47 mL/h) and slightly lower in muscle (0.10 vs. 0.12 mL/h). Nevertheless, the measured lymph flows serves as reliable input values for the PBPK model and foster critical evaluation of previously used values. This also suggests that flow is highly tissue-specific and might not be well-captured by fixing it to a given fraction of the respective plasma flow for all tissues. The lymph flow values we employed here based on our *in vivo* washout assessment correspond to 1.9% and 0.17% of the plasma flow (Table 2) in the skin and muscle, respectively.

The PBPK modelling approach showed that for tissues with very limited or very quick extravasation, estimation of parameters for antibody distribution to or removal from the interstitial space is not feasible based on the biodistribution data, despite extensive and early sampling times. The model structure did therefore not include distribution to and removal from the interstitial space for these tissues either antibody distribution was restricted to the vascular space in the case of very tight capillary structures or the plasma and interstitial space were lumped as one extracellular distribution space in tissues with discontinuous capillaries. For the

tissues with discontinuous capillaries, the biophase concentration would hence follow the plasma concentration levels. The amount of drug measured in the brain and kidney was explainable solely by the expected drug in the residual plasma of these tissues. It should be noted, though, that if corrective factors for residual plasma are fixed values that are too low, the model would be forced to describe the remaining unexplained antibody content by estimation of distribution to and removal from the interstitial space. For tissues with continuous capillaries, measured interstitial and residual plasma fractions were used and a tissue distribution flow was estimated in the model, allowing a detailed description of the biodistribution data. Overall, this is a relatively simple PBPK modelling approach compared to many of the more detailed previously published PBPK models (e.g., (Ferl *et al.*, 2005; Garg & Balthasar, 2007; Urva *et al.*, 2010; Chen & Balthasar, 2012). It is worthwhile noting, however, our intention here to keep the model complexity rather low while permitting for a realistic prediction of the biophase concentration within in the different tissues. Therefore, and to avoid unnecessary complexity and parameter identifiability issues, we omitted processes where experimental data were lacking. We acknowledge, though, that depending on the research question, more detailed model structures, including additional processes, could be necessary (e.g., target binding, FcRn receptors, endosomal compartment, etc.). It is of interest that the herein presented data and parameter values offer essential information on tissue composition, antibody target-site distribution and parameter identifiability independently from the model structure and could be integrated into other PBPK models.

In conclusion, we have provided novel data essential for PBPK modelling of monoclonal antibodies. To our knowledge, this is the first time that a PBPK model has been used to directly describe measured tissue interstitial PK for monoclonal antibodies. The measured input parameters, their direct integration and the critical evaluation of the measured and previously used values, as well as the underlying experimental methods, are vital for a more realistic interpretation of tissue PK data for antibodies. This allows us to model antibody tissue distribution and removal in a more tissue-specific way based on physiological rationale. We show that the use of residual plasma correction factors based on red blood cell distribution can lead to errors in estimation of extravascular antibody concentrations. Most importantly, we

demonstrate by direct measurements and model-based data interpretation that in most tissues, high interstitial concentrations can be achieved for antibodies that contradicts the still-prevailing view that antibody distribution to the tissue interstitial space is quite limited and low concentrations are expected. These findings also supply new insights with a potential impact on the development of IgG therapeutics. They show that the use of total tissue concentrations of antibodies can be highly misleading and does not reflect how much of the therapeutic antibody potentially reaches its target in the interstitial space. Correlating this concentration to a therapeutic effect could therefore bias the estimated potency of the respective antibody drug, and potential *in vitro - in vivo* correlation or upfront predictions of drug effect would be biased. The model developed herein offers a more precise prediction of the distribution of IgG antibodies to the interstitial space of individual tissues. These predicted target-site concentrations might be utilised to better assess the PKPD relationship and potency of antibody therapeutics. This knowledge could then potentially be further employed to more accurately predict expected PK and the therapeutic effect of IgG antibody agents upfront, also following alternative dosing schedules.

We believe that our findings are broadly applicable for IgG monoclonal antibodies which currently are the primary isotype for therapeutic antibodies. However, we recognise that differences in physicochemical properties, e.g., hydrodynamic radius or charge, for other Ig isotypes or engineered antibodies might affect certain distribution properties of protein therapeutics (e.g., passage through the endothelial layer or exclusion volume in the interstitial space). Investigating the impact of such factors on specific PK parameters during future studies, specifically combining experiments with PBPK modelling, could ultimately be a valuable next step to improve PBPK modelling for antibody therapeutics.

References

Aukland K & Reed RK. (1993). Interstitial-lymphatic mechanisms in the control of extracellular fluid volume. *Physiol Rev* **73,** 1-78.

Baxter LT, Zhu H, Mackensen DG & Jain RK. (1994). Physiologically based pharmacokinetic model for specific and nonspecific monoclonal antibodies and fragments in normal tissues and human tumor xenografts in nude mice. *Cancer Res* **54,** 1517-1528.

Boswell CA, Bumbaca D, Fielder PJ & Khawli LA. (2012). Compartmental tissue distribution of antibody therapeutics: experimental approaches and interpretations. *Aaps J* **14,** 612-618.

Boswell CA, Mundo EE, Ulufatu S, Bumbaca D, Cahaya HS, Majidy N, Van Hoy M, Schweiger MG, Fielder PJ, Prabhu S & Khawli LA. (2014). Comparative physiology of mice and rats: radiometric measurement of vascular parameters in rodent tissues. *Molecular pharmaceutics* **11,** 1591-1598.

Brown RP, Delp MD, Lindstedt SL, Rhomberg LR & Beliles RP. (1997). Physiological parameter values for physiologically based pharmacokinetic models. *Toxicology and industrial health* **13,** 407-484.

Chen Y & Balthasar JP. (2012). Evaluation of a catenary PBPK model for predicting the in vivo disposition of mAbs engineered for high-affinity binding to FcRn. *Aaps J* **14,** 850-859.

Covell DG, Barbet J, Holton OD, Black CD, Parker RJ & Weinstein JN. (1986). Pharmacokinetics of monoclonal immunoglobulin G1, F(ab')2, and Fab' in mice. *Cancer Res* **46,** 3969-3978.

Danhof M, de Jongh J, De Lange EC, Della Pasqua O, Ploeger BA & Voskuyl RA. (2007). Mechanism-based pharmacokinetic-pharmacodynamic modeling: biophase distribution, receptor theory, and dynamical systems analysis. *Annu Rev Pharmacol Toxicol* **47,** 357-400.

Davda JP, Jain M, Batra SK, Gwilt PR & Robinson DH. (2008). A physiologically based pharmacokinetic (PBPK) model to characterize and predict the disposition of monoclonal antibody CC49 and its single chain Fv constructs. *Int Immunopharmacol* **8,** 401-413.

Deng R, Iyer S, Theil FP, Mortensen DL, Fielder PJ & Prabhu S. (2011). Projecting human pharmacokinetics of therapeutic antibodies from nonclinical data: what have we learned? *MAbs* **3,** 61-66.

Eigenmann MJ, Fronton L, Grimm HP, Otteneder MB & Krippendorff B. (2017). Quantification of IgG monoclonal antibody clearance in tissues. *mAbs; DOI: 101080/1942086220171337619*.

Ferl GZ, Theil FP & Wong H. (2016). Physiologically based pharmacokinetic models of small molecules and therapeutic antibodies: a mini-review on fundamental concepts and applications. *Biopharm Drug Dispos* **37,** 75-92.

Ferl GZ, Wu AM & DiStefano JJ, 3rd. (2005). A predictive model of therapeutic monoclonal antibody dynamics and regulation by the neonatal Fc receptor (FcRn). *Ann Biomed Eng* **33,** 1640-1652.

Fronton L, Pilari S & Huisinga W. (2014). Monoclonal antibody disposition: a simplified PBPK model and its implications for the derivation and interpretation of classical compartment models. *J Pharmacokinet Pharmacodyn* **41,** 87-107.

Fung YC. (1993). *Biomechanics, Mechanical Properties of Living Tissues*. Springer Verlag, New York Inc.

Garg A. (2007). Investigation of the role of FcRn in the absorption, distribution and elimination of

monoclonal antibodies. In *Department of Pharmaceutical Sciences*. State University of New York at Buffalo.

Garg A & Balthasar JP. (2007). Physiologically-based pharmacokinetic (PBPK) model to predict IgG tissue kinetics in wild-type and FcRn-knockout mice. *J Pharmacokinet Pharmacodyn* **34,** 687-709.

Goldsmith HL, Cokelet GR & Gaehtgens P. (1989). Robin Fahraeus: evolution of his concepts in cardiovascular physiology. *Am J Physiol* **257,** H1005-1015.

Grundy D. (2015). Principles and standards for reporting animal experiments in The Journal of Physiology and Experimental Physiology. *J Physiol* **593,** 2547-2549.

Jones HM, Mayawala K & Poulin P. (2013). Dose selection based on physiologically based pharmacokinetic (PBPK) approaches. *Aaps J* **15,** 377-387.

Karlsen TV, McCormack E, Mujic M, Tenstad O & Wiig H. (2012). Minimally invasive quantification of lymph flow in mice and rats by imaging depot clearance of near-infrared albumin. *Am J Physiol Heart Circ Physiol* **302,** H391-401.

Lindena J, Kupper W & Trautschold I. (1986). Catalytic enzyme activity concentration in thoracic duct, liver, and intestinal lymph of the dog, the rabbit, the rat and the mouse. Approach to a quantitative diagnostic enzymology, II. Communication. *J Clin Chem Clin Biochem* **24,** 19-33.

Lobo ED, Hansen RJ & Balthasar JP. (2004). Antibody pharmacokinetics and pharmacodynamics. *J Pharm Sci* **93,** 2645-2668.

Mariappan TT, Mandlekar S & Marathe P. (2013). Insight into tissue unbound concentration: utility in drug discovery and development. *Curr Drug Metab* **14,** 324-340.

Michel CC & Curry FE. (1999). Microvascular permeability. *Physiol Rev* **79,** 703-761.

Modi S, Stanton AW, Mortimer PS & Levick JR. (2007). Clinical assessment of human lymph flow using removal rate constants of interstitial macromolecules: a critical review of lymphoscintigraphy. *Lymphat Res Biol* **5,** 183-202.

Mouton JW, Theuretzbacher U, Craig WA, Tulkens PM, Derendorf H & Cars O. (2008). Tissue concentrations: do we ever learn? *J Antimicrob Chemother* **61,** 235-237.

Pierson RN, Jr., Price DC, Wang J & Jain RK. (1978). Extracellular water measurements: organ tracer kinetics of bromide and sucrose in rats and man. *Am J Physiol* **235,** F254-264.

Rippe B & Haraldsson B. (1994). Transport of macromolecules across microvascular walls: the two-pore theory. *Physiol Rev* **74,** 163-219.

Sarin H. (2010). Physiologic upper limits of pore size of different blood capillary types and another perspective on the dual pore theory of microvascular permeability. *J Angiogenes Res* **2,** 14.

Shah DK & Betts AM. (2012). Towards a platform PBPK model to characterize the plasma and tissue disposition of monoclonal antibodies in preclinical species and human. *J Pharmacokinet Pharmacodyn* **39,** 67-86.

Shah DK & Betts AM. (2013). Antibody biodistribution coefficients: inferring tissue concentrations of monoclonal antibodies based on the plasma concentrations in several preclinical species and human. *MAbs* **5,** 297-305.

Tsuji A, Yoshikawa T, Nishide K, Minami H, Kimura M, Nakashima E, Terasaki T, Miyamoto E, Nightingale CH & Yamana T. (1983). Physiologically based pharmacokinetic model for beta-lactam antibiotics I: Tissue distribution and elimination in rats. *J Pharm Sci* **72,** 1239-1252.

Urva SR, Yang VC & Balthasar JP. (2010). Physiologically based pharmacokinetic model for T84.66: a monoclonal anti-CEA antibody. *J Pharm Sci* **99,** 1582-1600.

Valentin J. (2002). Guide for the practical application of the ICRP Human Respiratory Tract Model. A report of ICRP supporting guidance 3: approved by ICRP committee 2 in October 2000. *Annals of the ICRP* **32,** 13-306.

Wan H. (2016). An overall comparison of small molecules and large biologics in ADME testing. *ADMET & DMPK* **4,** 1-22.

Wang W, Wang EQ & Balthasar JP. (2008). Monoclonal antibody pharmacokinetics and pharmacodynamics. *Clin Pharmacol Ther* **84,** 548-558.

Wiig H, Aukland K & Tenstad O. (2003). Isolation of interstitial fluid from rat mammary tumors by a centrifugation method. *Am J Physiol Heart Circ Physiol* **284,** H416-424.

Wiig H & Swartz MA. (2012). Interstitial fluid and lymph formation and transport: physiological regulation and roles in inflammation and cancer. *Physiol Rev* **92,** 1005-1060.

Wiig H, Tenstad O & Bert JL. (2005). Effect of hydration on interstitial distribution of charged albumin in rat dermis in vitro. *J Physiol* **569,** 631-641.

Additional information

Competing interests

Ludivine Fronton is now employed at Bayer AG. The findings and conclusions in this work are those of the authors and do not necessarily represent the view of Bayer AG. Other than this, the authors declare no competing interests in relation to the work described here.

Author contribution

M.J.E. - Contributed to the design and conception of the work, as well as the acquisition, analysis and interpretation of the data; also drafted and revised the work for important intellectual content.

T.V.K. - Contributed to the acquisition, analysis and interpretation of the data; revised the work for important intellectual content.

B.K. - Contributed to the analysis and interpretation of the data; revised the work for important intellectual content.

O.T. - Contributed to the acquisition, analysis and interpretation of the data; revised the work for important intellectual content.

L.F. - Contributed to the design and conception of the work; revised the work for important intellectual content.

M.B.O. - Contributed to the conception of the work and interpretation of the data; revised the work for important intellectual content.

H.W. – Contributed to the design and conception of the work, as well as acquisition, analysis and interpretation of the data; drafted and revised the work for important intellectual content.

All authors approved the final version of the manuscript and agreed to be accountable for all aspects of the work to ensure that questions related to the accuracy or integrity of any part of it are appropriately investigated and resolved. All authors designated as authors qualify for

authorship, and those who are eligible for authorship are listed.

Funding

Financial support from The Research Council of Norway (project #262079 to HW) is gratefully acknowledged.

Acknowledgments

We would like to thank Gerd S. Salvesen and Åse R. Eriksen for all their technical support during the experimental studies. Moreover, we would like to acknowledge the support of Sherri Dudal in the planning of this work.

Tables

Table 1: Subcompartmental volume fractions in tissues

Tissue	Adipose	Bone	Brain	Gut	Heart	Kidney	Liver	Lung	Muscle	Skin	Spleen
fECV	0.101	0.176	-	0.197	0.210	-	0.333	0.364	0.137	0.448	0.184
CV (%)	*42.9*	*15.0*	-	*14.9*	*19.3*	-	*15.6*	*11.7*	*25.3*	*7.9*	*20.8*
fResPla	0.007	0.043	0.012	0.022	0.086	0.108	0.094	0.137	0.009	0.017	0.065
CV (%)	*47.8*	*14.1*	*22.7*	*27.8*	*19.2*	*10.9*	*15.7*	*16.7*	*15.5*	*30.6*	*26.0*
fVint	0.093	0.133	-	0.175	0.123	-	0.239	0.227	0.127	0.431	0.119
CV (%)	*46.2*	*20.3*	-	*17.1*	*35.8*	-	*22.6*	*21.1*	*27.6*	*8.4*	*35.3*

Table 1: Measured extracellular (fECV), residual plasma volume fractions (fResPla) and derived interstitial volume fractions (fVint) in mL/g tissue presented as mean and coefficient of variation (CV) for all 11 tissues.

Table 2: Parameter values used in the PBPK model

Tissue-specific parameters							
Tissue	***fResPla (mL/g)*** [a]	***Tissue dist. (mL/h)*** [b]	***Lymph flow (mL/h)*** [b]	***Frct. CL*** [c]	***Organ volume (mL)*** [d]	***fVint (mL/g)*** [e]	***Plasma flow (mL/h)*** [d]
Adipose	0.006 (± 1.7e-5)	0.001 (± 5.9e-6)	0.005 (± 3.9e-5)	0.027	1.775	0.093	11.7
Bone	0.024 (± 7.9e-5)	0.007 (± 9.9e-5)	0.041 (± 5.6e-4)	0.100	2.525	0.133	13.3
Brain	0.012 (± 1.7e-5)	-	-	0.001	0.425	-	10.4
Gut	0.023 (± 1.1e-4)	0.031 (± 2.0e-4)	0.212 (± 7.2e-4)	0.026	1.050	0.175	65.4
Heart	0.070 (± 1.7e-4)	0.004 (± 9.1e-5)	0.020 (± 4.1e-4)	0.005	0.135	0.123	31.8
Kidney	0.101 (± 1.3e-4)	-	-	0.060	0.470	-	59.6
Liver	0.082 (± 1.1e-4)	-	-	0.300	1.725	-	9.1
Lung	0.118 (± 2.7e-5)	0.002 (± 2.4e-5)	0.005 (± 5.7e-5)	0.013	0.183	0.227	324
Muscle	0.007 (± 2.7e-5)	0.034 (± 1.5e-4)	0.124[f] (± 5.7e-4)	0.190	10.1	0.130	74.8

Skin	0.014 (± 8.3e-5)	0.107 (± 1.6e-4)	0.467[f] (± 3.7e-4)	0.250	4.475	0.430	24.3
Spleen	0.061 (± 8.7e-5)	-	-	0.028	0.125	-	7.1

Other parameters						
Syst. Vpla (mL)[b]	***Total CL (mL/h)[b]***	***CO plasma (mL/h)[d]***	***Frct. access. skin[b]***	***Frct. access. muscle[b]***	***fResPla skin cent.[a]***	***fResPla muscle cent.[a]***
0.793 (± 7.9e-5)	0.009 (± 2.9e-5)	324	0.634 (± 0.001)	0.748 (± 0.002)	0.065	0.056

Table 2: Summary of the parameter values used and estimated for the PBPK modelling approach. (a) Estimated but restricted to the range of the measured values ± 20%; (b) Estimated values; (c) Fixed values based on (Eigenmann et al., 2017), note: bone and adipose assumed; (d) Relative values derived from Shah et al. (Shah & Betts, 2012) and scaled to a 25g mouse; (e) Fixed to measured values; f) estimated but restricted to the range of the measured values ± 30%. The 95% confidence intervals (CI) for the parameters estimates are defined in brackets below the estimated value with the upper and lower bound of the 95% CI being defined as the estimate + or – the value in the bracket, respectively. A narrow confidence interval indicates a precise estimation of the respective model parameters. Definitions: residual plasma fraction (fResPla), tissue distribution (Tissue dist.), fractional contribution to total systemic clearance (Frct.CL), interstitial volume fraction (fVint), systemic plasma volume (Syst. Vpla), total systemic clearance (Total CL), plasma cardiac output (CO plasma), accessible volume fraction in interstitial space (Frct. access.) and residual plasma fraction in tissue centrifugate (fResPla cent.).

Figure legends

Figure 1: a) Schematic model structure. Solid arrows depict the blood flows and the dashed arrows indicate leaving of the tissue interstitial space (grey) indicates the lymph flow (where estimable). The tissues are modelled depending on their vasculature and are depicted again separately in the sub-plots, including the respective tissue-specific model parameters; (b) Tissues with continuous capillaries (green); (c) Tissues with capillaries largely impenetrable for IgGs, i.e., brain and kidney (orange); and (d) Tissues discontinuous capillaries (blue). The tissue-specific model parameters are: arterial plasma flow (Q_{tis}), lymph flow (L_{tis}), intrinsic clearances (CL_{tis}), residual plasma volume (Vv_{tis}) and the interstitial volume (Vi_{tis}). The venous blood flow is defined by (Q_{tis}-L_{tis}).

Figure 2: Individual (open circles) and mean (solid lines) anti-IL17 IgG total concentrations in plasma and the 11 tissues harvested at 10 time points over 15 days. Each profile is a composite profile, i.e., each individual data point was measured in a different mouse. Also shown in each sub-plot is a detailed zoom-in plot of the initial phase (0.6 d) of the concentration-time experiment.

Figure 3: Concentration of anti-IL17 IgG in the isolated fluid of the muscle and skin as a function of time after injection. Open circles indicate individual measurements (three mice per time point) and the solid curve is the mean profile. A detailed zoom-in plot of the initial phase (0.6 d) of the concentration-time experiment is found in both subplots.

Figure 4: a) Measured ^{51}Cr-EDTA spaces for different tissues in six mice. Individual volumes are reported per gram wet weight and mean and standard deviation are shown for each tissue; and b) Depiction of residual plasma fractions remaining in the tissues after harvesting. Individual measurement data, their mean and standard deviation are given for each tissue.

Figure 5: Measured total tissue PK profiles (solid profile with mean and standard deviation) corrected for amount of drug in residual

plasma assessed as ^{125}I-albumin distribution volume (solid red curve) and anti-IL17 IgG distribution volume (dashed red curve) after 5 and 10 min of circulation time, respectively. The blue-shaded area shows anticipated extravascular antibody concentration after accounting for the drug content in the calculated tracer distribution spaces. The size of the blue-shaded area is defined by the difference in the volume fraction assessed by ^{125}I-albumin distribution after 5 min and ^{125}I-anti-IL17 IgG distribution after 10min.

Figure 6: Measured total tissue PK profiles (solid profile with mean and standard deviation) corrected for amount of drug in residual plasma assessed as ^{125}I-albumin distribution volume (solid red curve) and anti-IL17 IgG distribution volume (dashed red curve) after 5 and 10 min of circulation time respectively. In these tissues no or very low extravascular tissue concentrations were expected after accounting for the drug in the assessed tracer spaces (blue-shaded area). The size of the blue-shaded area is defined by the difference in the volume fraction assessed by ^{125}I-albumin distribution after 5min and ^{125}I-anti-IL17 IgG distribution after 10 min.

Figure 7: Measured removal rates in skin (filled) and muscle (open) for BSA, normal IgG antibody and FcRn non-binding IgG, respectively. Washout rates (in 1/h) were 0.32±0.06, 0.31±0.09 and 0.36±0.05 in skin and 0.13±0.03, 0.11±0.05 and 0.14±0.04 in muscle for BSA, IgG and FcRn non-binding IgG, respectively.

Figure 8: Model description of the biodistribution data. The model prediction is shown as the black solid line. The fitted mean PK data are represented by the open circles. Amount of drug in the residual plasma of the tissues is depicted in red, in interstitial fluid with the in blue-dashed lines and where not distinguishable in green.

Figure 9: Overview of the sensitivities of the model outputs (y-axis) on perturbations in the individual parameters (x-axis). The sensitivity was averaged over the entire simulated time-course of 360 h. Yellow indicates high- and dark blue low impact of changes in the parameters on the respective model output. The colour-code is presented on the scale on the right side of the figure.

Figure 10: Total tissue PK in tissues corrected for amount of drug in residual plasma in harvested tissues. Residual plasma volumes are determined based on either red blood cell distribution volumes reported by Garg (2007; green-dashed) and Boswell (2014; green-solid) and converted to plasma using a haematocrit value of 0.45 or by directly assessing the plasma space with labelled HSA (solid red) and IgG (dashed orange). It is clearly demonstrated that the red blood cell-based method leads systematically to lower correction and thus higher expected extravascular concentrations in tissues (grey-shaded area) than when directly assessed with plasma tracers (blue-shaded area).

Appendix

Parameter definitions

A_{tis} = Amount in tissue

Ai_{tis} = Amount in tissue interstitial space

Av_{tis} = Amount in tissue residual plasma

C_{tis} = Total tissue concentration

$Cint_{tis}$ = Tissue interstitial concentration

CL_{intpla} = Total systemic clearance

fCL_{tis} = Fractional contribution to clearance

L_{tis} = Tissue lymph flow

Q_{tis} = Tissue arterial plasma flow

Inflow = Antibody tissue distribution flow

V_{pla} = Systemic plasma volume

V_{tis} = Total tissue volume

Vi_{tis} = Tissue interstitial volume

Vv_{tis} = Tissue residual plasma volume

Model differential equations

Plasma

$$\frac{dA_{pla}}{dt} = \frac{L_{bon} \times Ai_{bon}}{Vi_{bon}} - \frac{Q_{bon} \times A_{pla}}{V_{pla}} + \frac{(Q_{lun} - L_{lun}) \times Av_{lun}}{Vv_{lun}} + \frac{L_{lun} \times Ai_{lun}}{Vi_{lun}} - \frac{Qa_{liv} \times A_{pla}}{V_{pla}} - \frac{Q_{ski} \times A_{pla}}{V_{pla}} + \frac{L_{ski} \times Ai_{ski}}{Vi_{ski}} - \frac{Q_{mus} \times A_{pla}}{V_{pla}} + \frac{L_{mus} \times Ai_{mus}}{Vi_{mus}} - \frac{Q_{spl} \times A_{pla}}{V_{pla}} - \frac{Q_{gut} \times A_{pla}}{V_{pla}} + \frac{L_{gut} \times Ai_{gut}}{Vi_{gut}} - \frac{Q_{kid} \times A_{pla}}{V_{pla}} - \frac{Q_{hea} \times A_{pla}}{V_{pla}} + \frac{L_{hea} \times Ai_{hea}}{Vi_{hea}} - \frac{Q_{adi} \times A_{pla}}{V_{pla}} - \frac{Q_{bra} \times A_{pla}}{V_{pla}} + \frac{L_{adi} \times Ai_{adi}}{Vi_{adi}}$$

Adipose

Vascular:

$$\frac{dAv_{adi}}{dt} = -\frac{Inflow_{adi} \times Av_{adi}}{Vv_{adi}} + \frac{Q_{adi} \times A_{pla}}{V_{pla}} - \frac{(Q_{adi} - L_{adi}) \times Av_{adi}}{Vv_{adi}} - \frac{Av_{adi}}{Vv_{adi}} \times CL_{intpla} \times fCL_{adi}$$

Interstitial:

$$\frac{dAi_{adi}}{dt} = \frac{Inflow_{adi} \times Av_{adi}}{Vv_{adi}} - \frac{L_{adi} \times Ai_{adi}}{Vi_{adi}}$$

Bone

Vascular:

$$\frac{dAi_{bon}}{dt} = \frac{Inflow_{bon} \times Av_{bon}}{Vv_{bon}} - \frac{L_{bon} \times Ai_{bon}}{Vi_{bon}}$$

Interstitial:

$$\frac{dAv_{bon}}{dt} = -\frac{Inflow_{bon} \times Av_{bon}}{Vv_{bon}} + \frac{Q_{bon} \times A_{pla}}{V_{pla}} - \frac{(Q_{bon} - L_{bon}) \times Av_{bon}}{Vv_{bon}} - \frac{Av_{bon}}{Vv_{bon}} \times CL_{intpla} \times fCL_{bon}$$

Brain

$$\frac{dA_{bra}}{dt} = \frac{Q_{bra} \times A_{pla}}{V_{pla}} - \frac{Q_{bra} \times Av_{bra}}{Vv_{bra}} - \frac{Av_{bra}}{Vv_{bra}} \times CL_{intpla} \times fCL_{bra}$$

Gut

Vascular:

$$\frac{dAp_{gut}}{dt} = -\frac{Inflow_{gut} \times Av_{gut}}{Vv_{gut}} + \frac{Q_{gut} \times A_{pla}}{V_{pla}} - \frac{(Q_{gut} - L_{gut}) \times Av_{gut}}{Vv_{gut}} - \frac{Av_{gut}}{Vv_{gut}} \times CL_{intpla} \times fCL_{gut}$$

Interstitial:

$$\frac{dAi_{gut}}{dt} = \frac{Inflow_{gut} \times Av_{gut}}{Vv_{gut}} - \frac{L_{gut} \times Ai_{gut}}{Vi_{gut}}$$

Heart

Vascular:

$$\frac{dAv_{hea}}{dt} = \frac{Q_{hea} \times A_{pla}}{V_{pla}} - \frac{Inflow_{hea} \times Av_{hea}}{Vv_{hea}} - \frac{(Q_{hea} - L_{hea}) \times Av_{hea}}{Vv_{hea}} - \frac{Av_{hea}}{Vv_{hea}} \times CL_{intpla} \times fCL_{hea}$$

Interstitial:

$$\frac{dAi_{hea}}{dt} = \frac{Inflow_{hea} \times Av_{hea}}{Vv_{hea}} - \frac{L_{hea} \times Ai_{hea}}{Vi_{hea}}$$

Kidney

$$\frac{dA_{kid}}{dt} = \frac{Q_{kid} \times A_{pla}}{V_{pla}} - \frac{Q_{kid} \times Av_{kid}}{Vv_{kid}} - \frac{Av_{kid}}{Vv_{kid}} \times CL_{intpla} \times fCL_{kid}$$

Liver

$$\frac{dA_{liv}}{dt} = \frac{Qa_{liv} \times A_{pla}}{V_{pla}} - \frac{(Qa_{liv} + Q_{gut-}L_{gut} + Q_{spl}) \times A_{liv}}{Vd_{liv}} + \frac{Q_{spl} \times A_{spl}}{Vd_{spl}} + \frac{(Q_{gut-}L_{gut}) \times Av_{gut}}{Vv_{gut}} - \frac{Av_{liv}}{Vd_{liv}} \times CL_{intpla} \times fCL_{liv}$$

Lung

Vascular:

$$\frac{dAv_{lun}}{dt} = -\frac{Inflow_{lun} \times Av_{lun}}{Vv_{lun}} - \frac{(Q_{lun-}L_{lun}) \times Av_{lun}}{Vv_{lun}} + \frac{(Q_{bon-}L_{bon}) \times Av_{bon}}{Vv_{bon}} + \frac{(Q_{liv} + Q_{gut-}L_{gut} + Q_{spl}) \times A_{liv}}{Vv_{liv}} + \frac{(Q_{ski-}L_{ski}) \times Av_{ski}}{Vv_{ski}} + \frac{(Q_{mus-}L_{mus}) \times Av_{mus}}{Vv_{mus}} + \frac{Q_{kid} \times Av_{kid}}{Vv_{kid}} + \frac{(Q_{hea-}L_{hea}) \times Av_{hea}}{Vv_{hea}} + \frac{(Q_{adi-}L_{adi}) \times Av_{adi}}{Vv_{adi}} + \frac{Q_{bra} \times Av_{bra}}{Vv_{bra}} - \frac{Av_{lun}}{Vv_{lun}} \times CL_{intpla} \times fCL_{lun}$$

Interstitial:

$$\frac{dAi_{lun}}{dt} = \frac{Inflow_{lun} \times Av_{lun}}{Vv_{lun}} - \frac{L_{lun} \times Ai_{lun}}{Vi_{lun}}$$

Muscle

Vascular:

$$\frac{dAv_{mus}}{dt} = \frac{Q_{mus} \times A_{pla}}{V_{pla}} - \frac{Inflow_{mus} \times Av_{mus}}{Vv_{mus}} - \frac{(Q_{mus-}L_{mus}) \times Av_{mus}}{Vv_{mus}} - \frac{Av_{mus}}{Vv_{mus}} \times CL_{intpla} \times fCL_{mus}$$

Interstitial:

$$\frac{dAi_{mus}}{dt} = \frac{Inflow_{mus} \times Av_{mus}}{Vv_{mus}} - \frac{L_{mus} \times Ai_{mus}}{Vi_{mus}}$$

Skin

Vascular:

$$\frac{dAi_{ski}}{dt} = \frac{Inflow_{ski} \times Av_{ski}}{Vv_{ski}} - \frac{L_{ski} \times Ai_{ski}}{Vi_{ski}}$$

Interstitial:

$$\frac{dAv_{ski}}{dt} = \frac{Q_{ski} \times A_{pla}}{V_{pla}} * fCL_{ski} - \frac{Inflow_{ski} \times Av_{ski}}{Vv_{ski}} - \frac{(Q_{ski} - L_{ski}) \times Av_{ski}}{Vv_{ski}} - \frac{Av_{ski}}{Vv_{ski}} \times CL_{intpla}$$

Spleen

$$\frac{dA_{spl}}{dt} = \frac{Q_{spl} \times A_{pla}}{V_{pla}} - \frac{Q_{spl} \times A_{spl}}{Vd_{spl}} - \frac{A_{spl}}{Vd_{spl}} \times CL_{intpla} \times fCL_{spl}$$

Model definitions

$$C_{pla} = \frac{A_{pla}}{V_{pla}}$$

$$C_{tis} = \frac{Ai_{tis} + Av_{tis}}{V_{tis}}$$

$$Cint_{ski} = \frac{\frac{Ai_{ski} + Ap_{ski}}{Vv_{ski}} \times fVpla_{cent_{ski}}}{Vi_{ski} \times faccess_{ski})}$$

$$Cint_{mus} = \frac{\frac{Ai_{mus} + Ap_{mus}}{Vv_{mus}} \times fVpla_{cent_{mus}}}{Vi_{mus} \times faccess_{mus})}$$

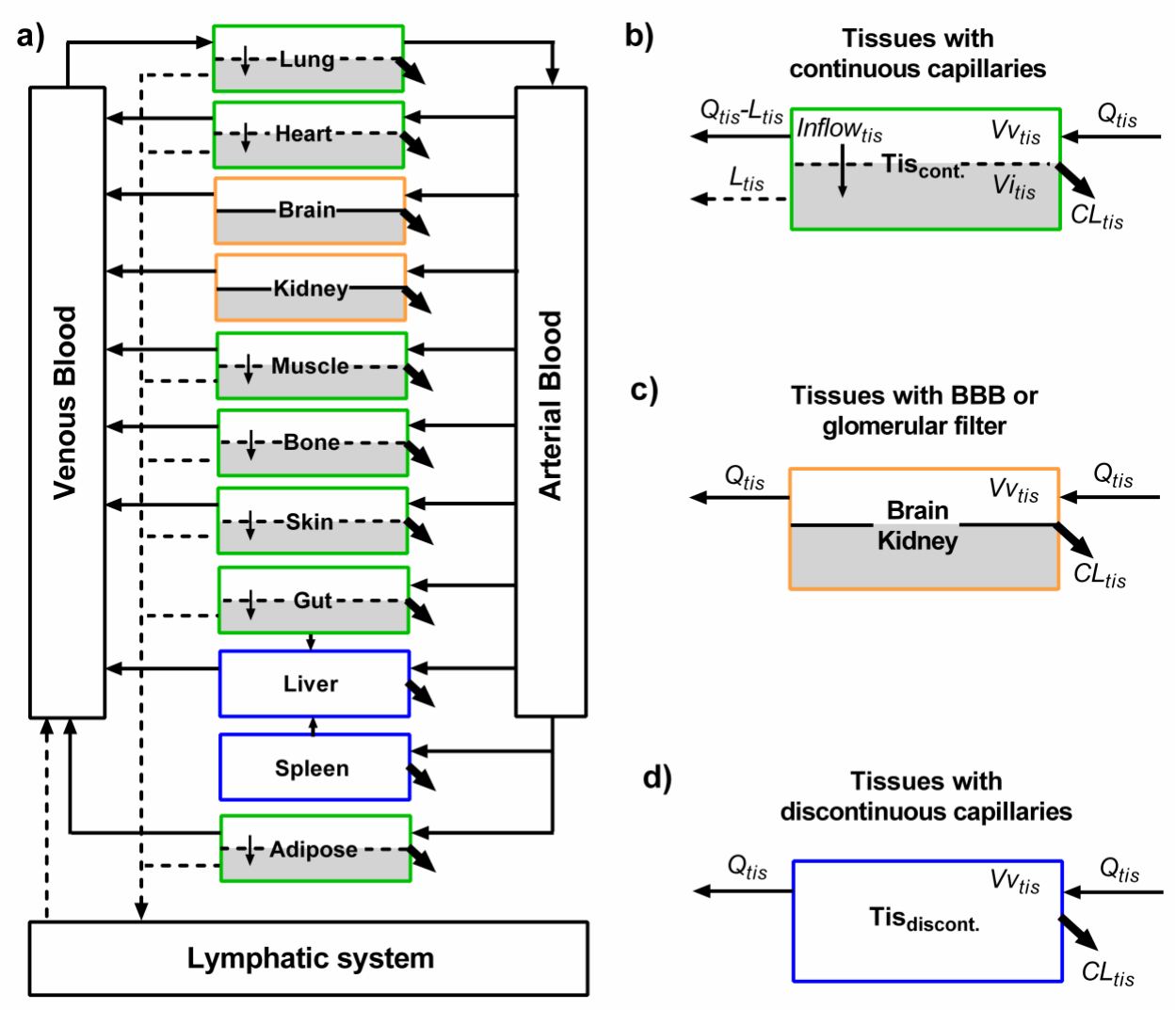
a)
Lung
Heart
Brain
Kidney
Muscle
Bone
Skin
Gut
Liver
Spleen
Adipose
Venous Blood
Arterial Blood
Lymphatic system
b)
Tissues with continuous capillaries
Q_{tis}-L_{tis}
$Inflow_{tis}$
Vv_{tis}
Q_{tis}
$Tis_{cont.}$
L_{tis}
Vi_{tis}
CL_{tis}
c)
Tissues with BBB or glomerular filter
Q_{tis}
Vv_{tis}
Q_{tis}
Brain
Kidney
CL_{tis}
d)
Tissues with discontinuous capillaries
Q_{tis}
Vv_{tis}
Q_{tis}
$Tis_{discont.}$
CL_{tis}

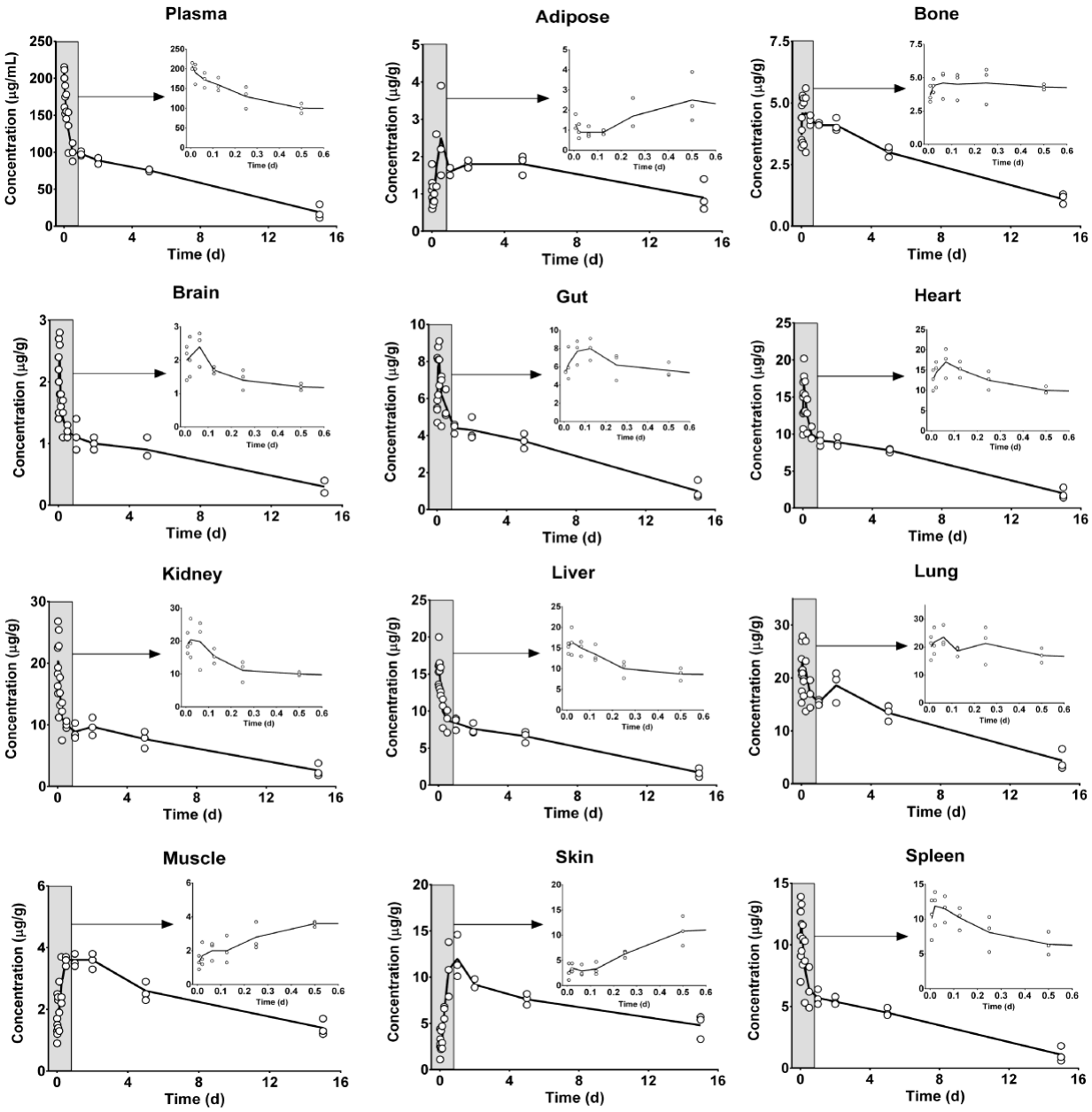
Plasma
Concentration (µg/mL)
Time (d)
Adipose
Concentration (µg/g)
Time (d)
Bone
Concentration (µg/g)
Time (d)
Brain
Concentration (µg/g)
Time (d)
Gut
Concentration (µg/g)
Time (d)
Heart
Concentration (µg/g)
Time (d)
Kidney
Concentration (µg/g)
Time (d)
Liver
Concentration (µg/g)
Time (d)
Lung
Concentration (µg/g)
Time (d)
Muscle
Concentration (µg/g)
Time (d)
Skin
Concentration (µg/g)
Time (d)
Spleen
Concentration (µg/g)
Time (d)

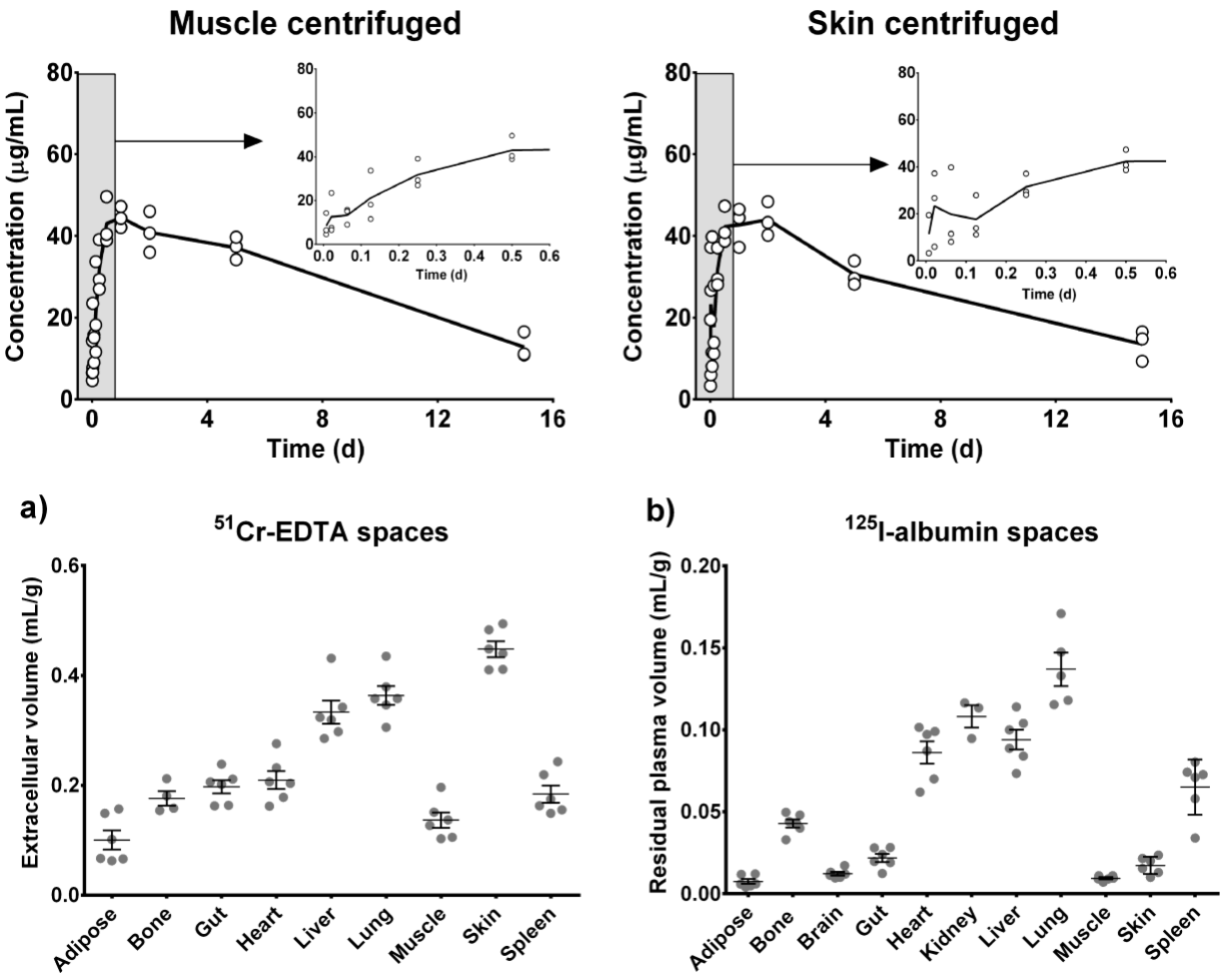
Muscle centrifuged
Skin centrifuged
Concentration (µg/mL)
Time (d)
a)
51Cr-EDTA spaces
Extracellular volume (mL/g)
Adipose
Bone
Gut
Heart
Liver
Lung
Muscle
Skin
Spleen
b)
125I-albumin spaces
Residual plasma volume (mL/g)
Adipose
Bone
Brain
Gut
Heart
Kidney
Liver
Lung
Muscle
Skin
Spleen

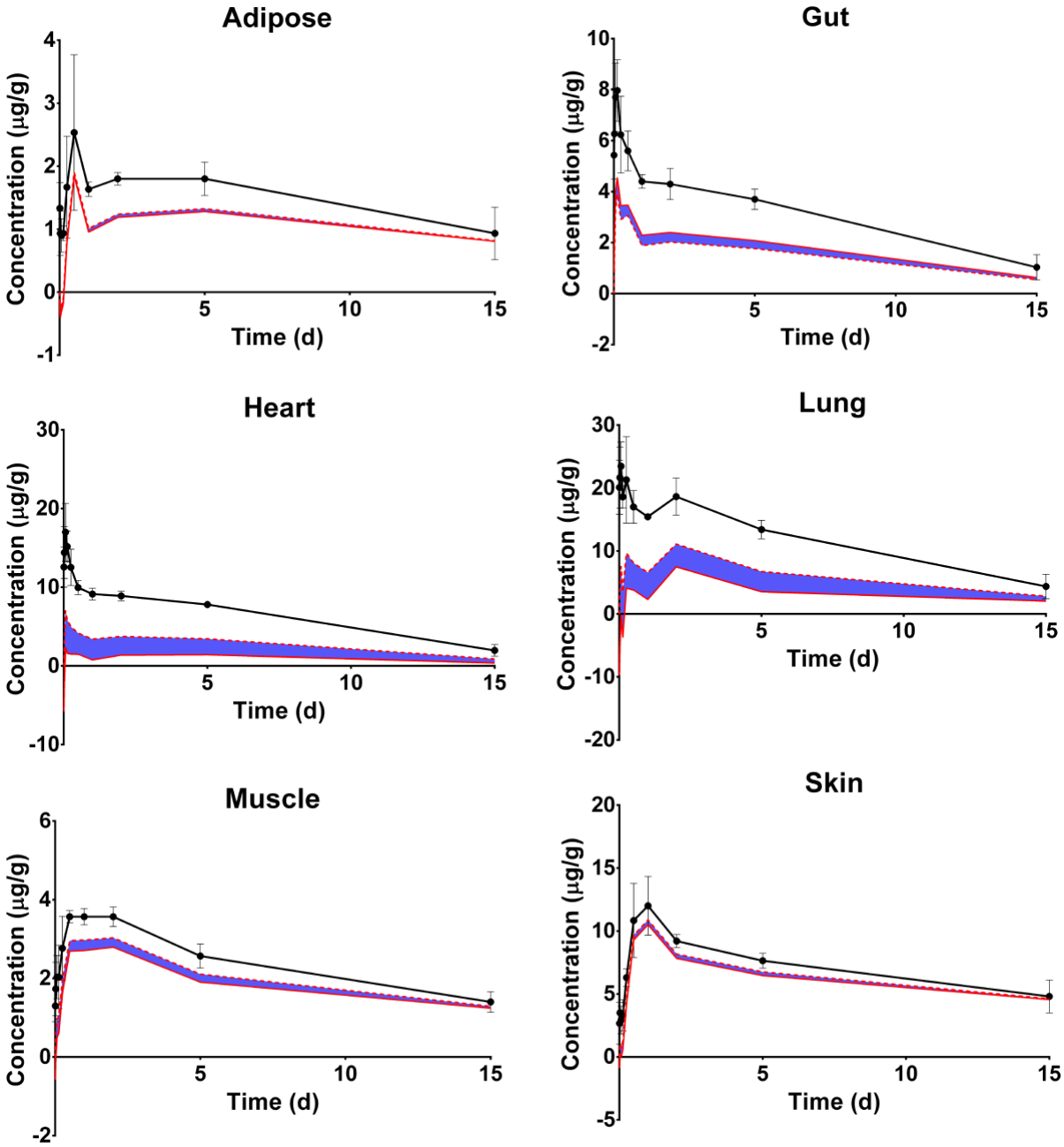
Adipose
Concentration (µg/g)
Time (d)
Gut
Concentration (µg/g)
Time (d)
Heart
Concentration (µg/g)
Time (d)
Lung
Concentration (µg/g)
Time (d)
Muscle
Concentration (µg/g)
Time (d)
Skin
Concentration (µg/g)
Time (d)

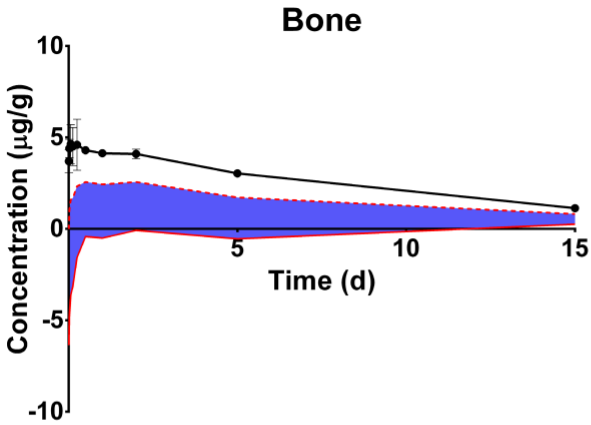
Bone
Concentration (µg/g)
Time (d)

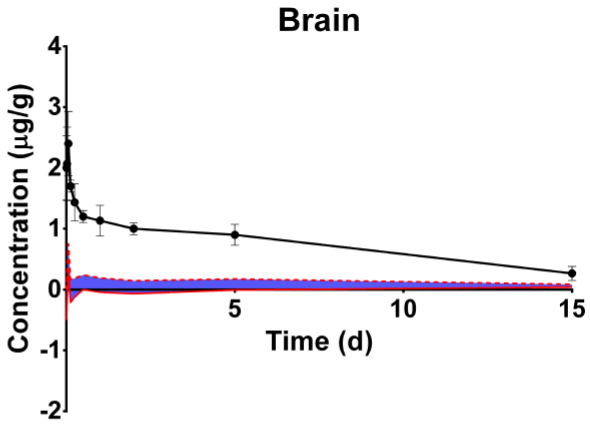
Brain
Concentration (µg/g)
Time (d)

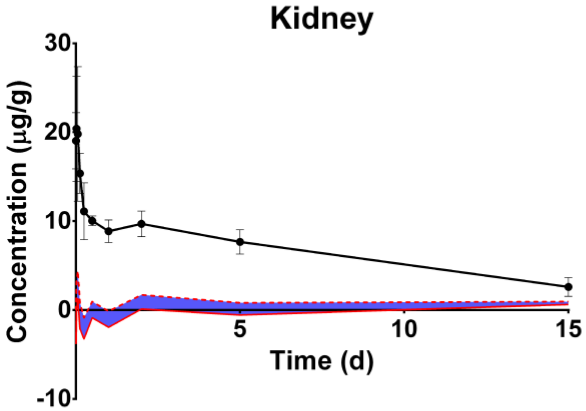
Kidney
Concentration (µg/g)
Time (d)

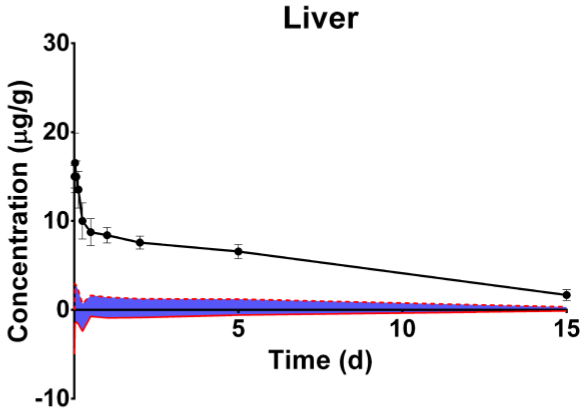
Liver
Concentration (µg/g)
Time (d)

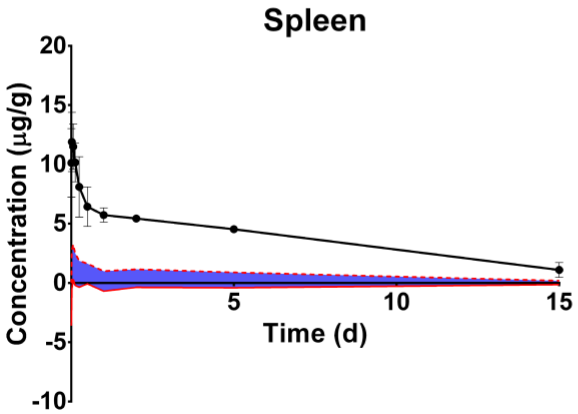
Spleen
Concentration (µg/g)
Time (d)

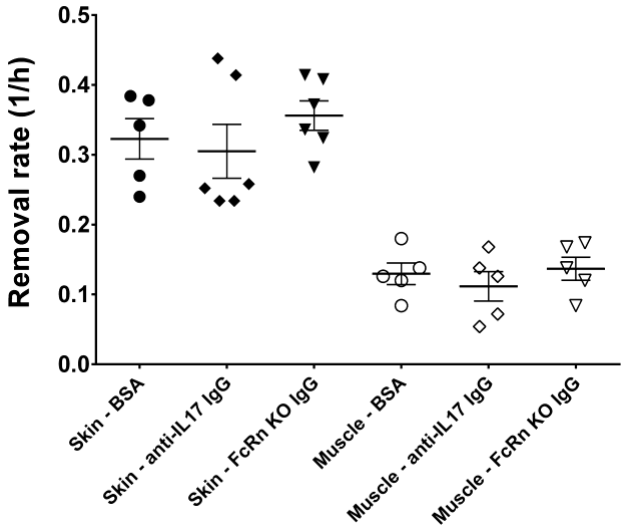
Removal rate (1/h)
0.5
0.4
0.3
0.2
0.1
0.0
Skin - BSA
Skin - anti-IL17 IgG
Skin - FcRn KO IgG
Muscle - BSA
Muscle - anti-IL17 IgG
Muscle - FcRn KO IgG

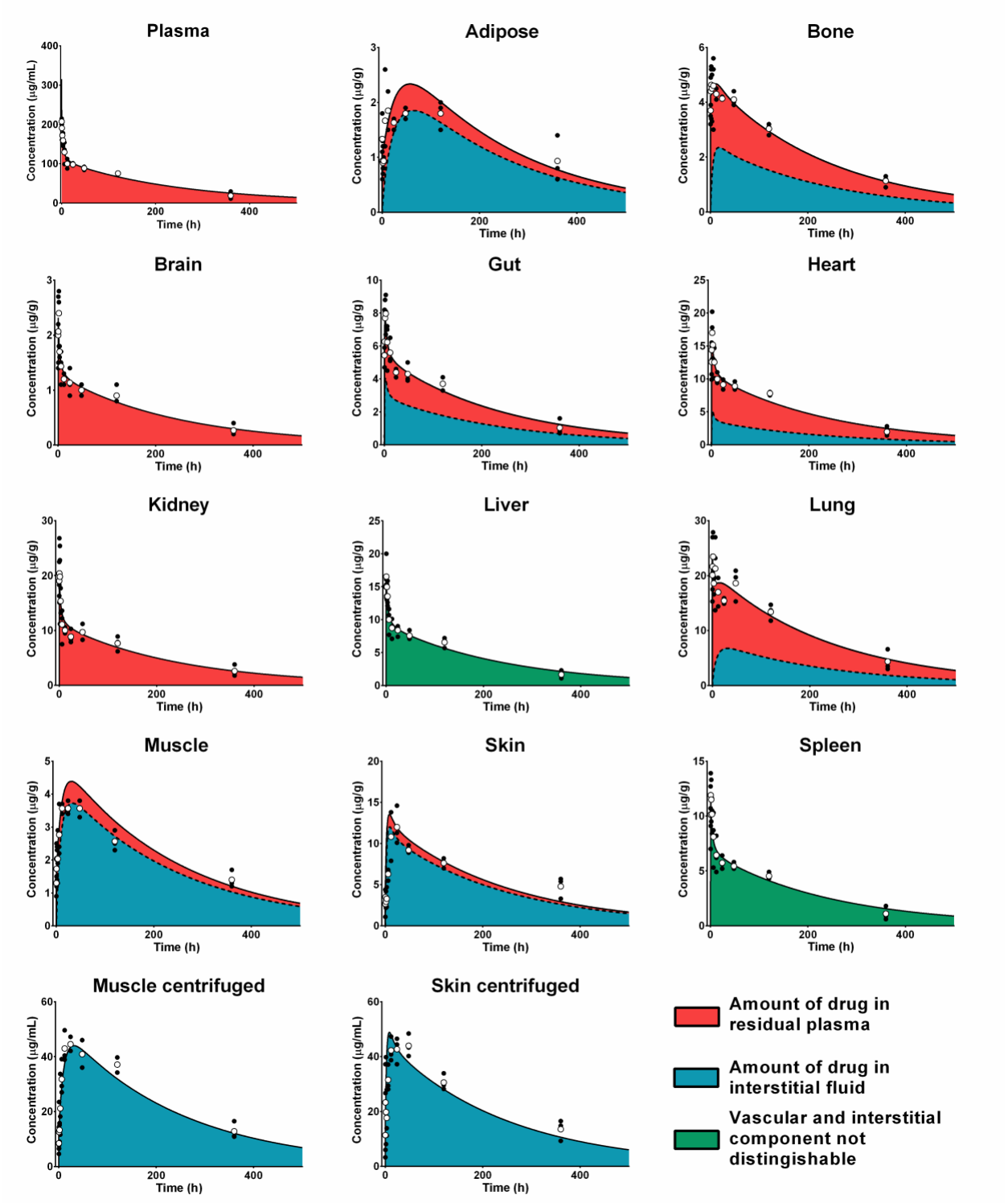
Plasma
Concentration (µg/mL)
Time (h)
Adipose
Concentration (µg/g)
Time (h)
Bone
Concentration (µg/g)
Time (h)
Brain
Concentration (µg/g)
Time (h)
Gut
Concentration (µg/g)
Time (h)
Heart
Concentration (µg/g)
Time (h)
Kidney
Concentration (µg/g)
Time (h)
Liver
Concentration (µg/g)
Time (h)
Lung
Concentration (µg/g)
Time (h)
Muscle
Concentration (µg/g)
Time (h)
Skin
Concentration (µg/g)
Time (h)
Spleen
Concentration (µg/g)
Time (h)
Muscle centrifuged
Concentration (µg/mL)
Time (h)
Skin centrifuged
Concentration (µg/mL)
Time (h)
Amount of drug in residual plasma
Amount of drug in interstitial fluid
Vascular and interstitial component not distingishable

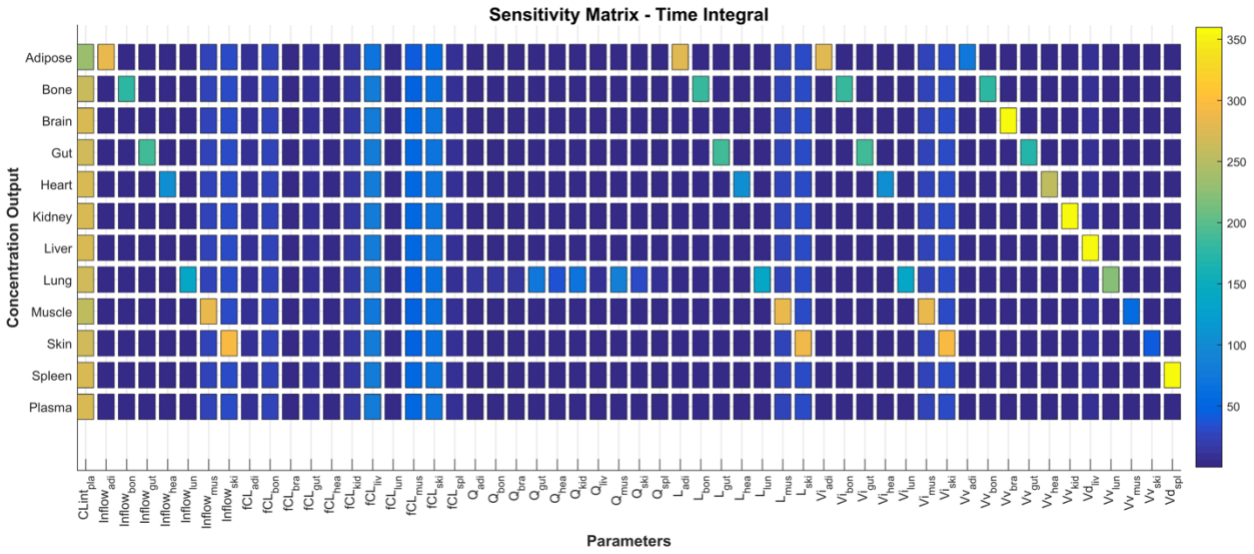
Sensitivity Matrix - Time Integral
Concentration Output
Adipose
Bone
Brain
Gut
Heart
Kidney
Liver
Lung
Muscle
Skin
Spleen
Plasma
Parameters
350
300
250
200
150
100
50

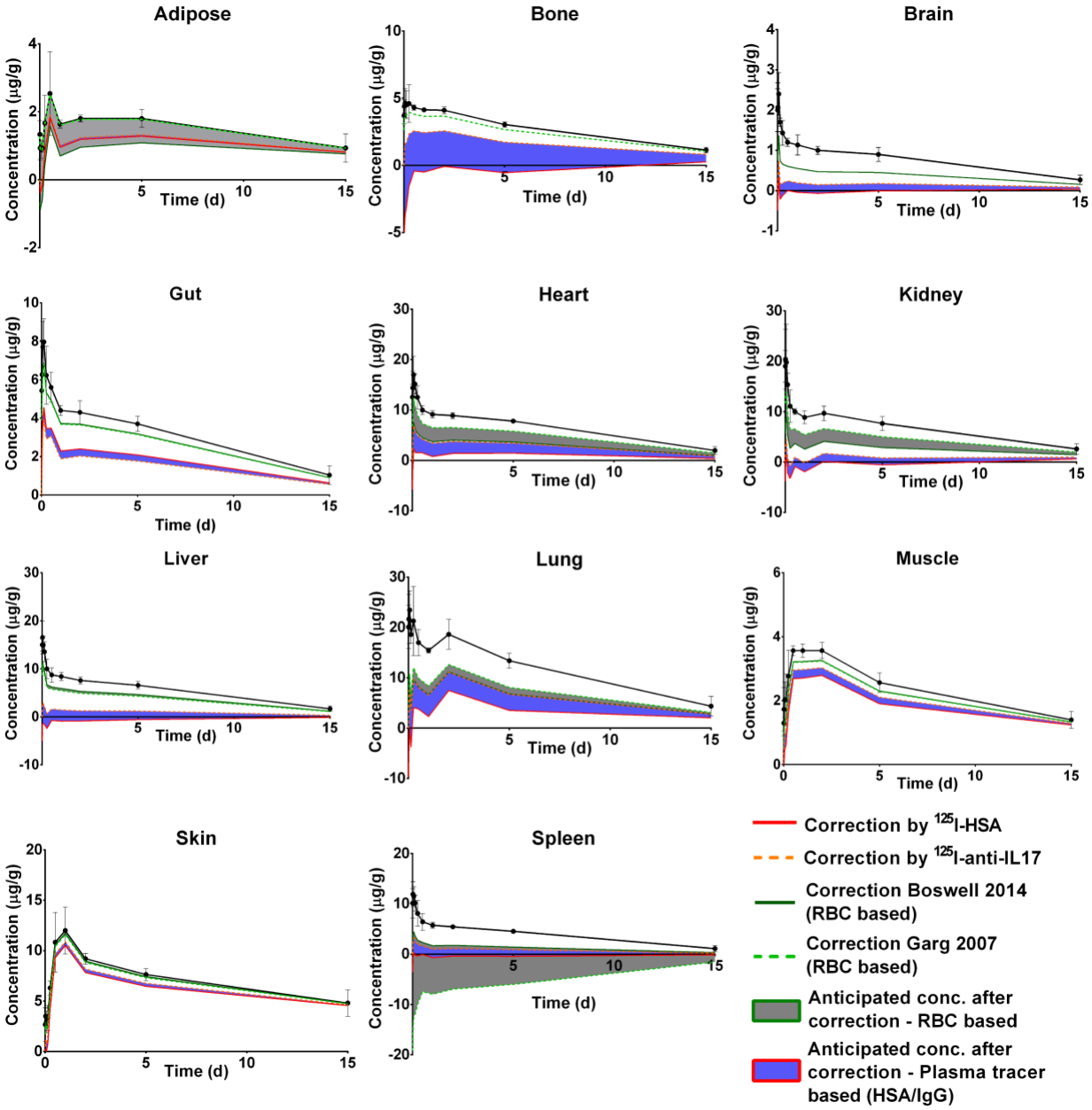
Adipose
Bone
Brain
Gut
Heart
Kidney
Liver
Lung
Muscle
Skin
Spleen
Concentration (µg/g)
Time (d)
Correction by 125I-HSA
Correction by 125I-anti-IL17
Correction Boswell 2014 (RBC based)
Correction Garg 2007 (RBC based)
Anticipated conc. after correction - RBC based
Anticipated conc. after correction - Plasma tracer based (HSA/IgG)